Applied Catalysis B: Environmental 187 (2016) 367–374

Contents lists available at ScienceDirect

Applied Catalysis B: Environmental

journal homepage: www.elsevier.com/locate/apcatb

Three-dimensional free-standing ZnO/graphene composite foam for photocurrent generation and photocatalytic activity

Xiaoju Men, Haobin Chen, Kaiwen Chang, Xiaofeng Fang, Changfeng Wu, Weiping Qin, Shengyan Yin*

State Key Laboratory on Integrated Optoelectronics, College of Electronic Science and Engineering, Jilin University, Changchun, Jilin 130012, China

ARTICLE INFO

Article history:
Received 17 November 2015
Received in revised form 21 January 2016
Accepted 23 January 2016
Available online 27 January 2016

Keywords:
Free-standing
Graphene foam
ZnO
Photocatalytic
Three-dimensional

ABSTRACT

A convenient, nontoxic and efficient way is developed for the fabrication of three-dimensional free-standing graphene foam modified with ZnO nanorods arrays. The resulting composite foam (ZnO/rGO foam) has a hierarchical micro-nano structure. The conductive macroporous structure will enhance the light harvesting, the photoinduced electron-hole separation and electrons transport. Moreover, the ZnO nanorods on the graphene surface will act as the active material which show the dramatic improvement in photocurrent generation and photocatalytic activity. This simple and scalable manufacturing technology will open a reasonable design and engineering route for the high-performance photoelectric conversion apparatus and environmental pollutant management.

1. Introduction

Fabrication of macroscopic structures with nanomaterials, while keeping the original properties of nano-building blocks, is of great significance to promote the practical applications. In the field of material science, graphene has received much attention because of its unique structure and its excellent physical and chemical properties, such as mechanical strength, big specific surface area, biocompatibility and chemical stability [1–6]. Integration of two-dimensional (2D) graphene nanosheets into a functional system is indispensable to investigate the advanced properties of individual graphene sheets for macroscopic applications [7–10]. Although many methods have been reported about assembling the graphene nanosheets into films or three-dimensional (3D) structures, interconnected 3D graphene foams have gained tremendous attention recently due to their unique structure and superior physical properties, which inherits from graphene sheets [11,12]. Based on functional graphene foams, many efforts have been made to enhance the performance of applications in sensing, energy conversion, environmental management, and catalysis [13,14]. To harness graphene foams for various applications, several approaches have been developed for fabrication of graphene foams, mainly including hydrothermal reduction of graphene oxides (GO), chemical reduction of GO, and chemical vapor deposition (CVD) growth on nickel foam skeletons [15]. As the precursor of graphene, GO can be obtained easily from graphite powders [16]. The introduced oxygen-containing groups can make pristine graphene water soluble, so that GO is a good candidate for the bottom-up assembly of graphene into macroscale materials [17]. Moreover, the graphene foam can be treated as a conductive 3D network substrate, which can be modified with other active material to meet the needs in different areas [18,19].

Photoelectric research has attracted a lot of attention from academic researchers and industry application engineers [20]. The main objective of photoelectric conversion is to obtain a good solar energy conversion efficiency. There are many factors associated with the efficiency, including light utilization efficiency, band gap of material used to build the device, separation efficiency of photoinduced electron-hole and photoinduced electrons transporting within the material freely, etc. Recently, we found that the 2D bio-inspired graphene composite porous structure were able to achieve high light utilization with low reflection, which resulted in improved photoelectric conversion [21]. The 3D graphene foam has deeper light penetration, and the light will scatter in the foam pore interior, which will reduce the reflective of the incident light. If there are active materials on the surface of the foam scaffold, the incident light will be maximally absorbed. The reasonable design and preparation of composite foams can help promote the sunlight utilization and improve the conversion efficiency. Furthermore, such a composite graphene foam is a good candidate as photocat-

* Corresponding author.
E-mail address: syyin@jlu.edu.cn (S. Yin).

http://dx.doi.org/10.1016/j.apcatb.2016.01.052
0926-3373/

alyst for the photodegradation of organic pollutants, which cause severe environmental and ecological problems every year [22–24].

Herein, in order to study the performance of the 3D graphene composite foam for photoelectric and photocatalytic application in energy or environment field [25,26], a simple, nontoxic and effective way is proposed to prepare a 3D free-standing composite graphene foam using Ni foam as the template and following a one-step hydrothermal process to form ZnO nanorods arrays capped on graphene surface. ZnO semiconducting material has been considered to be an ideal candidate for photoelectric and photocatalytic application due to its high electron mobility, nontoxicity and chemical stability [27–30]. In particular, the 3D self-supporting and hierarchical porous graphene structure acts as the conductive substrate which would let the solution pass through itself, and ZnO nanorods serve as the active material which can maximum exert dimensions and interfaces optimization. By combining the advantages of interconnected porous network, high conductivity, big surface area, good mechanical strength and thermal stability, the free-standing 3D graphene composite foams show high electrochemical activity and great potentialities for high-performance electrode materials in many energy conversion and photodegradation applications [31–34].

2. Experimental

2.1. Preparation of graphene oxide (GO)

A modified Hummers' method was used to prepare GO from natural graphite powder (Sigma) [35]. Briefly, graphite (1.1 g) was added into a solution of concentrated H_2SO_4 (8.6 mL), $K_2S_2O_8$ (1.8 g), and P_2O_5 (1.8 g). This solution was stirred at 80 °C for 6 h. After washed by deionized water, filtrated, and dried, the powder was added into another solution of concentrated H_2SO_4 (43.2 mL) and $KMnO_4$ (5.4 g). The mixture was stirred at 35 °C for 2 h. Then, 50 mL water was added into this mixture in an ice bath to keep the temperature below 50 °C. After further 2 h stirring, the solution was further diluted using water (100 mL), and then 5 mL of H_2O_2 (30%) was added into this solution to stop the reaction. The crude product was centrifuged and washed by HCl solution (V:V = 1:10, 300 mL), followed by repeated washing with water until the pH value is around neutral. The resulting product is graphite oxide. After ultrasonicated for 4 h, single layer graphene oxide suspensions were obtained by 30 min of 8000 rpm centrifugation.

2.2. Preparation of reduced graphene oxide foam (rGO foam)

The nickel foam (NF) was firstly washed by isopropanol, ethanol and deionized water for 5 min using an ultrasonic cleaner, respectively. In order to get free-standing 3D graphene foam, GO (C_{GO} = 3.1 mg/mL) suspension was dipped on the nickel foam (1.5 cm × 1.5 cm × 0.16 cm). In this step, we must ensure that GO solution was dipped evenly on the nickel surface of nickel foam. After GO/NF dried naturally, nickel foam coated with GO turned to yellow. The reduction of GO to reduced graphene oxide (rGO) was achieved by hydrazine reduced method. Briefly, GO/NF and 10 μL of hydrazine monohydrate were put into the autoclave and then heated the autoclave at 90 °C for 10 h to achieve the reduction of graphene oxide/nickel foam (rGO/NF). Finally, rGO/NF was immersed in the mixture of 0.5 M $FeCl_3$ and 1 M HCl solution for 5 h to remove nickel, and rGO foam was obtained. After washed and dialyzed with water several times, the three-dimensional, free-standing, and light-weight, rGO foam was formed. The pure rGO foam can be transferred onto quartz and ITO substrates for different applications, respectively.

2.3. Preparation of ZnO nanorods modified rGO foam (ZnO/rGO foam)

A modified Pacholski method was utilized to prepare ZnO nanocrystal seed [36]. Briefly, a NaOH ethanol solution (30 mM) and $(CH_3COO)_2Zn$ ethanol solution (10 mM) were mixed together slowly, and then the mixture solution was heated at 60 °C with stirring for 2 h. A few drops of the obtained spherical ZnO nanocrystal seed solution were added onto the rGO foam. After the ethanol solution dried, the ZnO seeds covered on the whole graphene surface of rGO foam. And then rGO foam was heated at 90 °C to make sure the ZnO seeds binding with rGO foam firmly. Then rGO foam which was supported on a substrate was put into an autoclave, at an angle around 30°, with the rGO side facing the bottom. The autoclave was filled with a solution containing $Zn(NO_3)_2{\cdot}6H_2O$ (30 mM) and hexamethylenetetramine (HMTA, 30 mM) and it was heated at 90 °C for 6 h to perform ZnO nanorods growth. After hydrothermal reaction completed, ZnO/rGO foam was rinsed with deionized water and then dried at room temperature.

A ZnO/rGO smooth film was also prepared using similar process. Briefly, GO aqueous solution was casted on a substrate, and dried naturally. After that, the GO film was reduced by hydrazine, and then followed the hydrothermal process to form ZnO nanorods arrays on graphene film surface as same condition as that of ZnO/rGO foam.

2.4. Photocurrent measurements

A three-electrode method was used to study the photocurrent properties with CHI 660D electrochemical station (CH Instruments). Here, rGO foam or ZnO/rGO foam acted as working electrode, Ag/AgCl as reference electrode (3.0 M KCl) and a Pt electrode as counter electrode. A 0.5 M Na_2SO_4 aqueous solution was chosen as electrolyte solution, and before testing, the electrolyte solution was purged for 60 min with nitrogen. A high-pressure Xe lamp was used as light source to simulate solar light. The light intensity was 100 mW/cm^2 and the area of the sample exposed to light was 1.5 cm^2.

2.5. Photocatalytic activity study

Rhodamine B (RhB) was used as a probe molecule to evaluate the photocatalytic activity of pure rGO foam, ZnO nanorod powder and ZnO/rGO foam. The absorbance spectra of RhB was measured with the same time interval, and the characteristic absorption peak of RhB at 554 nm was chosen to monitor the photocatalytic degradation process. The photocatalytic experiment was carried out by the following steps: Firstly, the RhB aqueous solution (5 ppm, 25 mL) was prepared, and then the catalyst was dispersed into this solution. The weight of the catalyst was controlled by the amount of ZnO nanorods, which was adjusted to be 0.2 mg/mL in all the photodegradation experiments. Before the photodegradation experiments, the mixture solution was placed in the dark with stirring for at least 30 min. This step is to sure that the RhB dye molecules are adsorption and desorption equilibrium on the surface of the corresponding catalysts. Secondly, a simulated solar light, whose flux intensity was 100 mW/cm^2, was used to irradiate the mixture solution. At each 10 min, 3 mL of mixture solution was taken out, and centrifuged at 6000 rpm for 10 min to remove the catalysts, and then the UV–vis absorbance spectra of the RhB aqueous solution was measured with a spectrophotometer (Shimadzu 3600). Here, the same amount of ZnO nanorods in the ZnO/rGO foam and pure ZnO nanorods powder was used to achieve the contrast experiments. Before the hydrothermal growth process, the weight of the rGO foam was measured. After the hydrothermal growth process, the weight of ZnO/rGO foam was also measured.

And then the weight of ZnO nanorods on the ZnO/rGO foam was obtained. According to the weight of ZnO on the ZnO/rGO foam, a suitable volume of RhB solution was chosen to keep the concentration of catalyst. Then, the same concentration of pure ZnO nanorods was used as the control.

2.6. Characterization methods

Scanning electron microscopy (SEM) images were collected on a JEOL JSM-7500F field emission scanning electron microscope. Raman spectra were recorded with a BWTEK Raman spectrophotometer with a 10 °C TE cooled linear array detector. 532 nm laser was used as the excited light source, and the spot size is about 1 μm. A Rigaku RU-200b X-ray powder diffractometer (XRD) was used to analyze the crystal structures using a nickel-filtered Cu-Kα radiation (λ = 0.15405 nm) in the range of $10^\circ \leq 2\theta \leq 70^\circ$. Total organic carbon (TOC) of initial and irradiated samples was determined with a Elementar vario TOC cube analyzer.

3. Results and discussion

3.1. Preparation and characterization of free-standing ZnO/rGO foam

The fabrication of 3D free-standing ZnO/rGO composite foam is illustrated in Fig. 1. Typically, the rGO foams can be prepared by immersing a piece of nickel foam (NF) (1.6 mm thick) in a suspension of GO (3.1 mg mL^{-1}). Then we dried the GO/NF under the ambient temperature. During the drying process, the surface of the nickel foam scaffold was covered by GO sheets. Then, the hydrazine vapour was utilized to reduce the resulting GO/NF foam. During this process, GO sheets were reduced and the obtained rGO was attached on the surface of the template scaffold. A solution contained ferric chloride ($FeCl_3$, 0.5 M) and hydrochloric acid (HCl, 1 M) was then used to remove nickel foam in the rGO/NF foam. After the nickel removal, the self-supporting rGO foam was formed. The graphene foam was formed by the strong π-π interaction of the adjacent graphene sheets when the GO was reduced to rGO, and then the firm rGO network will keep the graphene foam self-sporting. After we get the graphene foam, we fabricated densely packed ZnO nanorods arrays on the graphene surface. As described in the experimental section, we first prepared ZnO nanocrystal seed by the method of Pacholski et al. [36], and then we employed the seed onto the rGO foam framework. Finally, the ZnO nanorods grew through a hydrothermal growth method. Briefly, the rGO foam which was supported on a substrate was put into an autoclave, and a solution contained zinc nitrate and hexamethylenetetramine were utilized as the growth solution. When hydrothermal reaction completed, ZnO/rGO foam was rinsed with deionized water and then dried at room temperature. After the growth of ZnO nanorods, the ZnO/rGO foam is still self-supporting.

All the foam morphologies were studied by SEM (Fig. 2a–f). The representative SEM images of rGO/Ni foam are shown in Fig. 2a, which reveals that the obtained rGO/Ni foam exhibits a porous structure. After template removal, the top SEM image of rGO foam (Fig. 2b) clearly shows that rGO foam has a 3D interpenetrating porous structure and the pore size is about hundreds micrometers which is similar with that of the nickel foam, and the macropores in the rGO foam are connected with each other. The macroporous structure provided ample space to deposit active material with uniform penetration into the 3D structure interior. After ZnO nanorods growth, the ZnO/rGO foam keeps the structure of rGO foam (Fig. 2c). The macropores in the ZnO/rGO foam are exposed to the solution for the solution to go through it, and the target molecular can react not only at the surface of the foam but also in the foam interior. So that the free-standing graphene foam combines tractability, stiffness and mechanical flexibility which could be used in photocatalytic application. Fig. 2d and e shows the SEM images of ZnO nanorods on the graphene surface. It has been observed that the surface of the graphene in the foam was almost fully coated by ZnO nanorods (Fig. 2d). The ZnO nanorods have been thickly coated on the surface of ZnO/rGO foam scaffold without destroying the porous structure of the original rGO foam framework. In the higher magnified SEM image (Fig. 2e) and cross-sectional image of ZnO nanorods on the ZnO/rGO foam scaffold (Fig. 2f), it is observed that most of ZnO nanorods are perpendicular to the substrate [37], which will improve the light harvesting and also make the pollutant contact with the ZnO nanorods easily. Moreover, the diameter of ZnO nanorods is around 100 nm (inset of Fig. 2e), and the length is about 1.1 μm (Fig. 2f).

The successful preparation of ZnO/rGO foam was confirmed by Raman spectra and X-ray diffraction (XRD) measurements. There are two prominent Raman peaks at 1591 and 1346 cm^{-1} in the Raman spectrum of rGO foam, which can be ascribed to the well documented G and D bands of graphene, respectively (Fig. 3a, black line). The peak at about 1346 cm^{-1} (D band) is related to the defects and disorder in the hexagonal graphitic layers [38,39]. The I_D/I_G intensity ratio is an indicator of the disorder degree and average size of the sp^2 domains. Thus, it can be deduced that GO was reduced to rGO in the rGO foam after exposure to hydrazine vapor by the larger integral I_D/I_G ratio (Fig. 3a). Fig. 3b shows XRD results of ZnO/rGO foam. The sharp XRD peaks at 32.0°, 34.8°, 36.6°, 48.0°, 56.7°, 63.0°, 68.2° and 69.4° can be indexed to the (1 0 0), (0 0 2), (1 0 1), (1 0 2), (1 1 0), (1 0 3), (1 1 2) and (2 0 1), which can be accurately assigned to hexagonal ZnO (JCPDS file no. 80-0074), confirming that the samples are well crystallized hexagonal wurtzite-type and highly pure [29]. The broad peak at around 24° (approximately 3.70 Å) is close to the graphite peak, but the layer space is bigger than that of graphite (3.35 Å) [40]. This interlayer spacing is attributed to the reduction of the GO sheets.

3.2. Photocurrent generation

To characterize the antireflection effect of ZnO/rGO foam, the absorption and reflectance spectra of ZnO/rGO film, rGO foam and ZnO/rGO foam were tested. From the absorption spectra (Fig. 4a), rGO foam has an absorption peak at 260 nm; while ZnO/rGO film and ZnO/rGO foam have strong absorption below 400 nm, which is benefit from ZnO nanorods. The band gap energies can be estimated from UV–vis diffuse reflectance spectra. As shown in Fig. S1, the band gap of rGO foam and ZnO/rGO foam is 0.94 eV and 3.18 eV, respectively. The value of band gap is similar with the previous literature [41–44]. Beyond the absorption spectra, the reflectance spectra (Fig. 4b) shows that ZnO/rGO film (black curve) reflects 15% more of the incident light compared to ZnO/rGO foam (red curve). The refractive index of foam is different from that of the medium matrix, which may capture the light inside the pores by enhancing light scattering, and thus reduce incident light reflection. This properties may improve the light used in the composite foam and may result in the enhancement photoelectric and photocatalytic properties.

Photoelectric properties of these foams were investigated using electrochemical method. It was achieved in a Na_2SO_4 (0.5 M) electrolyte solution in a quartz cell, where the ZnO/rGO film, rGO foam or ZnO/rGO foam served as the working electrode, Pt electrode as the counter electrode, and Ag/AgCl electrode as the reference electrode [45]. I-V curves of rGO foam and ZnO/rGO foam devices in the absence and presence of irradiation by a continuous light are illustrated in Fig. 4c. An interesting increased photocurrent was observed. With illumination, rGO foam electrode showed a photocurrent starting from an almost negligible photocurrent at 0 V

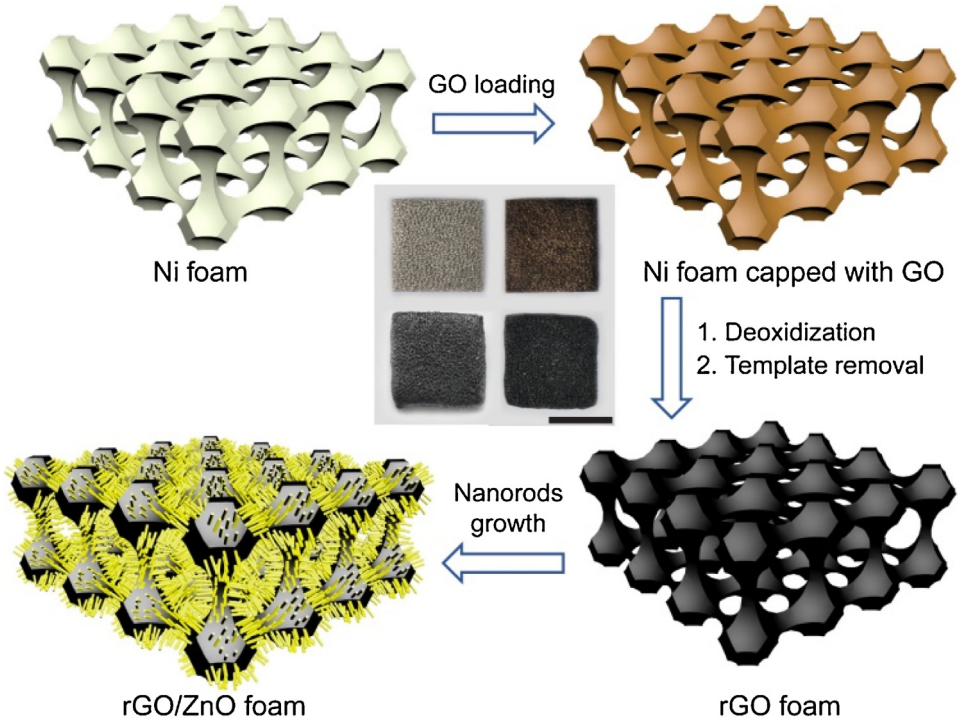

Fig. 1. Preparation schematic diagram of free-standing ZnO/rGO foam. Inset is the corresponding sample photographs of each step (the scale bar is 1 cm).

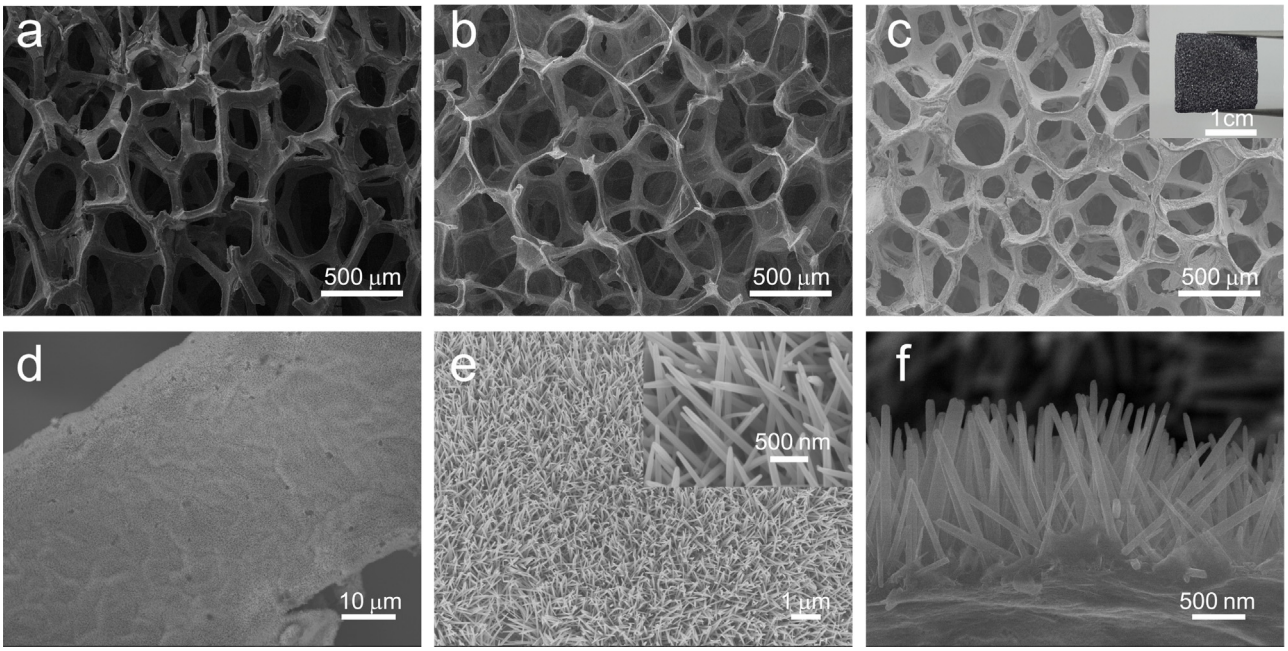

Fig. 2. SEM images of free-standing (a) rGO/Ni foam (b) rGO foam and (c) ZnO/rGO foam (inset is the photograph of free-standing ZnO/rGO foam); (d) SEM image of ZnO nanorods on the ZnO/rGO foam scaffold; (e) Magnified SEM images of ZnO nanorods on the ZnO/rGO foam (inset is the magnified SEM image of ZnO nanorods); and (f) Cross sectional image of ZnO nanorods on the ZnO/rGO foam scaffold.

and ending with 0.007 mA cm^{-2} at 1.0 V. In comparison, ZnO/rGO foam showed a pronounced photoresponse with a current density of 0.27 mA cm^{-2} at 1.0 V. Moreover, the photocurrent was not saturated even at high positive voltage, indicating the efficient charge separation in the hybrid foam. I-V curves confirm that the graphene porous structure combined with the active materials promotes the photoinduced electron-hole separation and electrons transport, and finally enhances the photocurrent generation.

The good performance of ZnO/rGO foam on photocurrent generation revealed that this composite foam was more sensitive to light irradiation. A swift and stable photocurrent of 0.041 mA cm^{-2} was detected for the ZnO/rGO foam, accompanied with alternating on-off cycles, when the potential of the ZnO/rGO foam electrode was set at 0 V (vs. Ag/AgCl) (Fig. 4d). The response of the on-off cycles was almost reversible. In comparison, the photocurrent generation of ZnO/rGO film electrode was much lower at 0.019 mA cm^{-2}; while the photocurrent generation of rGO foam electrode showed

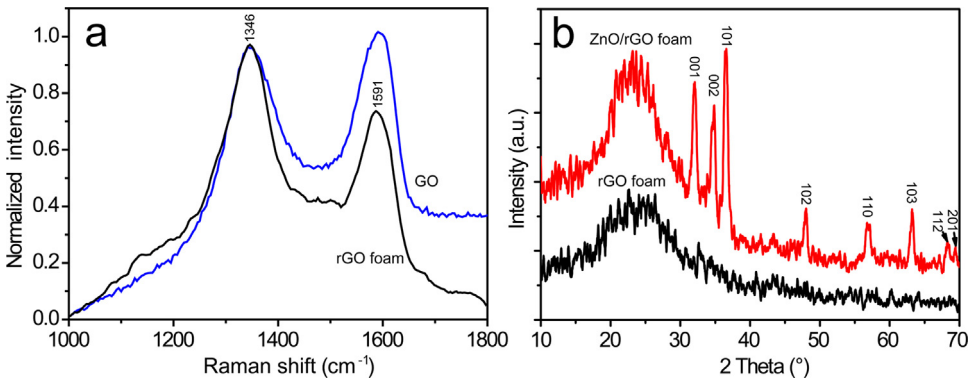

Fig. 3. (a) Raman spectra of rGO foam (black) and GO (blue) under the 532 nm laser excitation; (b) XRD spectra of free-standing rGO foam (black) and ZnO/rGO foam (red). (For interpretation of the references to colour in this figure legend, the reader is referred to the web version of this article).

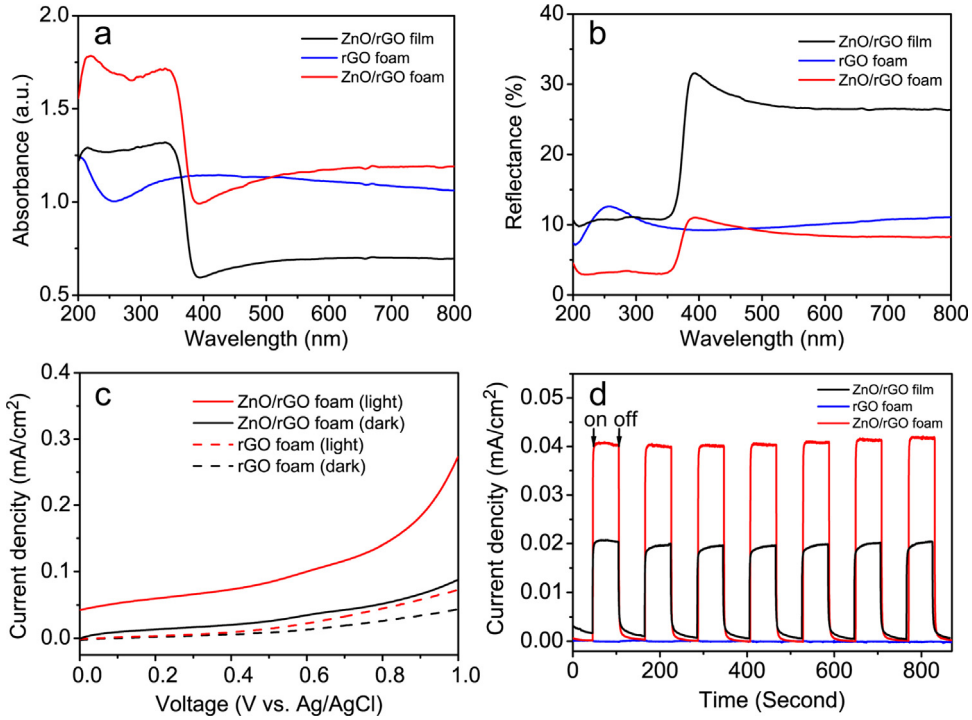

Fig. 4. (a) Absorption spectra and (b) reflectance spectra of ZnO/rGO film (black), rGO foam (blue), and ZnO/rGO foam (red), respectively; (c) I-V curves of rGO foam and ZnO/rGO foam with and without the illumination of a continuous simulated solar light from 0 V to 1.0 V; (d) Current versus time under chopped irradiation of ZnO/rGO film (black), rGO foam (blue) and ZnO/rGO foam (red) at a bias voltage of 0 V (vs. Ag/AgCl). (For interpretation of the references to colour in this figure legend, the reader is referred to the web version of this article).

almost negligent current (around 0 mA cm^{-2}). The composite photoelectrode, which consists of macroporous foam structure and active material, plays a significant role in the photocurrent generation. The light will scatter in the pore interior and the scatter light will continue to irradiate the active materials on the surface of the foam scaffold. Thus, ZnO/rGO foam could enhance the light utilization. Furthermore, as we know, the photocurrent from the illuminated semiconductor materials is determined by the speed of excited electrons transporting from semiconductor to conductivity substrate and the recombination at the electrolyte and semiconductor material interface. Herein, the 3D macroporous rGO foam structure serves good conductive substrate, which let electrons transport quickly and increase the separation efficiency of the photoinduced electron-hole pairs. Therefore, the ZnO/rGO foam shows good photoelectronic conversion properties due to the simultaneous improvement in light harvesting and charge transferring.

3.3. Photocatalytic activity

The ZnO/rGO foam which has large photocurrent density, big surface area and transparent pore structure could also be applied for photocatalytic applications. In order to investigate the photocatalytic degradation properties, Rhodamine B (RhB), a widely used model organic pollutant, was introduced. Ten slices of the ZnO/rGO foam (1.1 cm × 1.1 cm) were used while rGO foam and pure ZnO nanorods of the same amount were also applied as the control. 5 ppm RhB aqueous solution (25 mL) was used as the test solution. During the photodegradation process, the concentration change was characterized by the RhB absorption peak at 554 nm using an UV–vis spectrometer. The reaction solution was maintained in dark for 30 min and stirred at the same time to ensure adsorption-desorption equilibrium. The photocatalytic activity of pure RhB solution, rGO foam, ZnO nanorod powder and ZnO/rGO foam was evaluated as the reference under the same conditions.

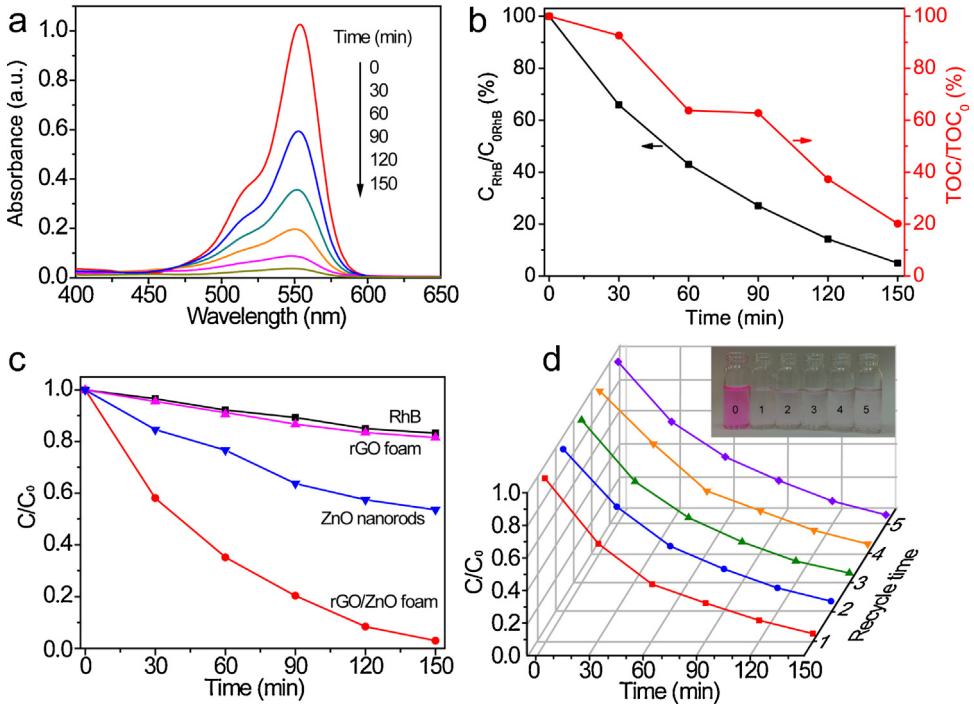

Fig. 5. (a) UV–vis spectra of RhB under illumination of a continuous simulated solar light for the same time interval with the ZnO/rGO foam; (b) Concentration change ratio of RhB (black curve) and TOC removal efficiency (red curve) during the same time interval in aqueous solution under illumination (C_{0RhB} and C_{RhB} are the concentration of RhB, which is evaluation by absorption peak of initial solution and photodegradation solution with different intervals, respectively; TOC_0 and TOC are the concentration of total organic carbon, which is evaluation by TOC of initial solution and photodegradation solution with different intervals, respectively); (c) Concentration change ratio of RhB under light illumination for same time interval with different substrates and the pure RhB under the same light illumination (C_0 and C are the concentration of RhB, which is evaluation by absorption peak of initial solution and photodegradation solution with different intervals, respectively), and (d) Recyclable photodegradation of the ZnO/rGO foam for the 1st, 2nd, 3rd, 4th and 5th cycles. (Inset is the images of RhB solution at initial (number 0) and at final (number 1–5) after every photodegradation recycles). (For interpretation of the references to colour in this figure legend, the reader is referred to the web version of this article).

The absorbance spectra of RhB during the photocatalytic degradation process by ZnO/rGO foam is shown in Fig. 5a. The concentration of RhB is decreased with time increasing under the illumination of a continuous simulated solar light. After 150 min illumination, the peak of RhB is almost disappeared, which indicates the low concentration of RhB. In order to further investigate the photodegradation of RhB, total organic carbon (TOC), which has been widely used to evaluate the degree of mineralization of organic species, was measured in the photodegradation process by ZnO/rGO foam under illumination. The results confirm that RhB is steadily mineralized by the as-prepared samples, as shown in Fig. 5b. Furthermore, the TOC residual ratio is 20.2% after 150 min illumination; while the concentration change ratio of RhB is 5.0%, which was form the data of UV–vis spectra. These data indicated that RhB was not degraded to CO_2 directly, and there were some intermediates [46,47]. Fig. 5c shows the photocatalytic properties of rGO foam absence and presence the assistance of ZnO nanorod using absorption spectra. The pure ZnO nanorods and no catalyst in the RhB solution were as the control. In the neutral RhB solution, pure RhB was relatively stable under the light illumination and only 16% was degraded over 150 min interval, while there is also similar degraded ratio by pure rGO foam. These show that the rGO foam has no photodegradation property. It is indicated that the degradation of RhB was very slow when there is no ZnO nanorods. The pure ZnO nanorods was also investigated under the same condition. In this case, about 46% of RhB was degradated at the same time interval. ZnO/rGO foam showed the best photocatalytic capability, and almost all the RhB (>95%) was decomposed in 150 min. Therefore, the photodegradation property was in good agreement with enhanced photocurrent generation. Significantly, graphene foams not only act as the substrate of ZnO nanorods but also play an outstanding role as an electron storage reservoir, leading to a high separation efficiency of the photoinduced electron-hole and an enhanced photocatalytic performance. When the photocatalytic experiment finished, the ZnO/rGO foams could be separated from the original reaction solution easily. We just need to remove ZnO/rGO foam from the reaction solution, wash it with deionized water and ethanol for several times to remove the organic residues on the foam surface, dry at nature temperature, and then this ZnO/rGO foam can be employed into another photocatalytic experiment. The recyclable photocatalytic degradation of RhB in the presence of the ZnO/rGO foam is illustrated in Fig. 5d. It is noted that during five recycles, the photocatalytic activity of ZnO/rGO foam is virtually efficient, indicating the potential of using the ZnO/rGO foam as a recyclable catalyst for the degradation of RhB under light irradiation.

Through the performance of photoelectric and photodegradation tests, Fig. 6 provides a possible mechanism for efficient electron-hole separation and electron transport at the ZnO/rGO foam. The active material ZnO nanorods are excited to generate electrons and holes under the light irradiation. The introduction of the rGO foam substrate provides a good electron transport route in the ZnO/rGO foam structure. The electrons in rGO foam could easily transfer from the conduction band ZnO nanorods, and enhance the separation efficiency of photogenerated electron-hole pairs. When there is an external circuit connected with the ZnO/rGO foam, there is a photocurrent obtained (as shown in Fig. 6, mechanism I). If there is no external circuit connected with the ZnO/rGO foam, the separated holes would directly react with RhB, or react with water to generate hydroxyl radicals. The radicals would subsequently oxidize the RhB due to their high oxidative capacity (as shown in Fig. 6, mechanism II). Therefore, the improvement of photoelectric performance and photocatalytic activity of the ZnO/rGO foam structure

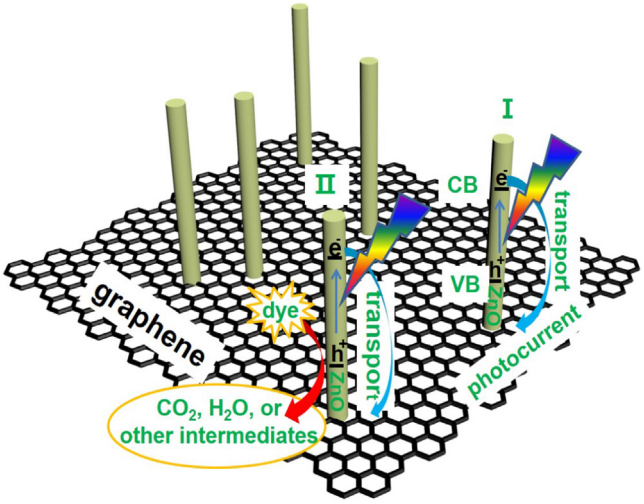

Fig. 6. Schematic illustration of the photocatalytic mechanism of the ZnO/rGO foam.

is mainly due to the high efficiency of photogenerated electron-hole separation, which induced by the high electron mobility of rGO foam.

Moreover, the improved photoelectric performance and photocatalysis performance of ZnO/rGO foam may also be attributed to following factors: (1) From the SEM images, we got the information that ZnO nanorods grew tightly on the graphene foam, so that the photoinduced electrons could quickly transport to the graphene substrate through a percolation process in the reaction system. Therefore, the separation efficiency of electron-hole pairs is improved, which will benefit for the enhancement in the photocatalytic activity obviously; (2) The large surface area of 3D graphene foam network allows more dye molecules to be adsorbed; (3) The macroporous structure with ZnO nanorods on the surface area enhances the light harvesting. The incident light will scatter in the macropore interior and the scatter light will continue to irradiate the ZnO nanorods on the graphene surface of the foam scaffold, which will enhance the light utilization; (4) ZnO/rGO foam was stable for the photodegradation [27–30]. Therefore, this photocatalyst material exhibits great suitability for the applications in water pollution with excellent stability and operational convenience.

4. Conclusions

In this work, we provided a convenient, nontoxic and efficient way for preparation of 3D self-supporting graphene foam using Ni foam as the template. By a one-step hydrothermal process, a compact, stable and homogeneous ZnO nanorods was prepared on the graphene surface. The resulting composite foam, ZnO/rGO foam, has a micro-nano hierarchical structure. This macroporous graphene scaffold will enhance the light harvesting and also help the light induced electron transport rapidly which promotes the separation efficiency of electron-hole. Such free-standing 3D graphene foam with ZnO nanorods not only has an increased photoelectric response, suggesting a substantial increase in a solar energy conversion efficiency of practical approach, but also demonstrate excellent performance during the degradation process. The direct, nontoxic, convenient and stable procedure for the fabrication of 3D free-standing graphene composite foam will open a great route for future applications of solar energy conversion and environmental pollutant management.

Acknowledgment

This work was supported by National Natural Science Foundation of China (NSFC) (Grants 51302103, 11474132 and 61335001), and Scientific and Technological Developing Project of Jilin Province (20140520101JH).

Appendix A. Supplementary data

Supplementary data associated with this article can be found, in the online version, at http://dx.doi.org/10.1016/j.apcatb.2016.01.052.

References

[1] F. Schedin, A.K. Geim, S.V. Morozov, E.W. Hill, P. Blake, M.I. Katsnelson, K.S. Novoselov, Nat. Mater. 6 (2007) 652–655.
[2] Y.W. Zhu, S. Murali, M.D. Stoller, K.J. Ganesh, W.W. Cai, P.J. Ferreira, A. Pirkle, R.M. Wallace, K.A. Cychosz, M. Thommes, D. Su, E.A. Stach, R.S. Ruoff, Science 332 (2011) 1537–1541.
[3] W. Gao, N. Singh, L. Song, Z. Liu, A.L.M. Reddy, L.J. Ci, R. Vajtai, Q. Zhang, B.Q. Wei, P.M. Ajayan, Nat. Nanotechnol. 6 (2011) 496–500.
[4] S. Park, N. Mohanty, J.W. Suk, A. Nagaraja, J.H. An, R.D. Piner, W.W. Cai, D.R. Dreyer, V. Berry, R.S. Ruoff, Adv. Mater. 22 (2010) 1736–1740.
[5] M.A. Worsley, P.J. Pauzauskie, T.Y. Olson, J. Biener, J.H. Satcher, T.F. Baumann, J. Am. Chem. Soc. 132 (2010) 14067–14069.
[6] N. Mahmood, C.Z. Zhang, H. Yin, Y.L. Hou, J. Mater. Chem. A 2 (2014) 15–32.
[7] S.Y. Yin, Z.Q. Niu, X.D. Chen, Small 8 (2012) 2458–2463.
[8] S.Y. Yin, Y. Zhang, J. Kong, C. Zou, C.M. Li, X. Lu, J. Ma, F.Y.C. Boey, X. Chen, ACS Nano 5 (2011) 3831–3838.
[9] H.M. Xu, H.C. Wang, C.P. Wu, N. Lin, A.M. Soomro, H.Z. Guo, C. Liu, X.D. Yang, Y.P. Wu, D.J. Cai, J.Y. Kang, Nanoscale 7 (2015) 10613–10621.
[10] J.T. Xu, M. Wang, N.P. Wickramaratne, M. Jaroniec, S.X. Dou, L.M. Dai, Adv. Mater. 27 (2015) 2042–2048.
[11] Y.N. Meng, Y. Zhao, C.G. Hu, H.H. Cheng, Y. Hu, Z.P. Zhang, G.Q. Shi, L.T. Qu, Adv. Mater. 25 (2013) 2326–2331.
[12] D.T. Pham, T.H. Lee, D.H. Luong, F. Yao, A. Ghosh, V.T. Le, T.H. Kim, B. Li, J. Chang, Y.H. Lee, ACS Nano 9 (2015) 2018–2027.
[13] P.P. Yu, X. Zhao, Z.L. Huang, Y.Z. Li, Q.H. Zhang, J. Mater. Chem. A 2 (2014) 14413–14420.
[14] H. Sun, P. She, K. Xu, Y. Shang, S. Yin, Z. Liu, Synth. Met. 209 (2015) 68–73.
[15] X. Cao, Y. Shi, W. Shi, G. Lu, X. Huang, Q. Yan, Q. Zhang, H. Zhang, Small 7 (2011) 3163–3168.
[16] Y.J. Wang, Q.S. Wang, X.Y. Zhan, F.M. Wang, M. Safdar, J. He, Nanoscale 5 (2013) 8326–8339.
[17] Y.C. Li, L. Zhang, Z.F. Hub, J.C. Yu, Nanoscale 7 (2015) 10896–10902.
[18] P. Pathak, S. Gupta, K. Grosulak, H. Imahori, V. Subramanian, J. Phys. Chem. C 119 (2015) 7543–7553.
[19] L. Yang, Z. Li, H. Jiang, W. Jiang, R. Su, S. Luo, Y. Luo, Appl. Catal. B: Environ. 183 (2016) 75–85.
[20] M. Seredych, O. Mabayoje, M.M. Kolesnik, V. Krstic, T.J. Bandosz, J. Mater. Chem. 22 (2012) 7970–7978.
[21] S.Y. Yin, X.J. Men, H. Sun, P. She, W. Zhang, C.F. Wu, W.P. Qin, X.D. Chen, J. Mater. Chem. A 3 (2015) 12016–12022.
[22] X.J. Liu, L.K. Pan, T. Lv, T. Lu, G. Zhu, Z. Sun, C.Q. Sun, Catal. Sci. Technol. 1 (2011) 1189–1193.
[23] Z.J. Zhang, W.Z. Wang, E.P. Gao, S.M. Sun, L. Zhang, J. Phys. Chem. C 116 (2012) 25898–25903.
[24] C. Han, Z. Chen, N. Zhang, J.C. Colmenares, Y.J. Xu, Adv. Funct. Mater. 25 (2015) 221–229.
[25] H. Sun, S. Liu, S. Liu, S. Wang, Appl. Catal. B: Environ. 146 (2014) 162–168.
[26] F. Perreault, A. Fonseca de Faria, M. Elimelech, Chem. Soc. Rev. 44 (2015) 5861–5896.
[27] D.L. Shao, H.T. Sun, J. Gao, G.Q. Xin, M.A. Aguilar, T.K. Yao, N. Koratkar, J. Lian, S. Sawyer, Nanoscale 6 (2014) 13630–13636.
[28] Y. Zhang, Z. Chen, S. Liu, Y.-J. Xu, Appl. Catal. B: Environ. 140–141 (2013) 598–607.
[29] D.P. Qi, L.Y. Zheng, X.B. Cao, Y.Y. Jiang, H.B. Xu, Y.Y. Zhang, B.J. Yang, Y.H. Sun, H.H. Hng, N. Lu, L.F. Chi, X.D. Chen, Nanoscale 5 (2013) 12383–12387.
[30] T.-T. Chen, I.C. Chang, M.-H. Yang, H.-T. Chiu, C.-Y. Lee, Appl. Catal. B: Environ. 142–143 (2013) 442–449.
[31] Y. Yang, L.L. Ren, C. Zhang, S. Huang, T.X. Liu, ACS Appl. Mater. Interfaces 3 (2011) 2779–2785.
[32] L. Xiao, D.Q. Wu, S. Han, Y.S. Huang, S. Li, M.Z. He, F. Zhang, X.L. Feng, ACS Appl. Mater. Interfaces 5 (2013) 3764–3769.
[33] J. Chen, K.X. Sheng, P.H. Luo, C. Li, G.Q. Shi, Adv. Mater. 24 (2012) 4569–4573.
[34] S.H. Choi, J.K. Lee, Y.C. Kang, Nano Res. 8 (2015) 1584–1594.
[35] W.S. Hummers Jr., R.E. Offeman, J. Am. Chem. Soc. 80 (1958) 1339.
[36] C. Pacholski, A. Kornowski, H. Weller, Angew. Chem. Int. Ed. 41 (2002) 1188–1191.

[37] S.Y. Yin, Y.L. Wu, B.H. Hu, Y. Wang, P.Q. Cai, C.K. Tan, D.P. Qi, L.Y. Zheng, W.R. Leow, N.S. Tan, S.T. Wang, X.D. Chen, Adv. Mater. Interfaces 1 (2014) 1300043.
[38] H.M. Zhang, X.Z. Yu, D. Guo, B.H. Qu, M. Zhang, Q.H. Li, T.H. Wang, ACS Appl. Mater. Interfaces 5 (2013) 7335–7340.
[39] J.F. Shen, Y.Z. Hu, C. Li, C. Qin, M. Shi, M.X. Ye, Langmuir 25 (2009) 6122–6128.
[40] X.C. Dong, Y.F. Cao, J. Wang, M.B. Chan-Park, L.H. Wang, W. Huang, P. Chen, RSC Adv. 2 (2012) 4364–4369.
[41] Y.C. Chen, D.G. de Oteyza, Z. Pedramrazi, C. Chen, F.R. Fischer, M.F. Crommie, ACS Nano 7 (2013) 6123–6128.
[42] S.A. Ansari, M.M. Khan, S. Kalathil, A. Nisar, J. Lee, M.H. Cho, Nanoscale 5 (2013) 9238–9246.
[43] Y. Shen, S.B. Yang, P. Zhou, Q.Q. Sun, P.F. Wang, L. Wan, J. Li, L.Y. Chen, X.B. Wang, S.J. Ding, D.W. Zhang, Carbon 62 (2013) 157–164.
[44] Z. Chen, N. Zhang, Y.J. Xu, CrystEngComm 15 (2013) 3022–3030.
[45] S.Y. Yin, Y. Goldovsky, M. Herzberg, L. Liu, H. Sun, Y. Zhang, F. Meng, X. Cao, D.D. Sun, H. Chen, A. Kushmaro, X. Chen, Adv. Funct. Mater. 23 (2013) 2972–2978.
[46] C. Han, M.Q. Yang, B. Weng, Y.J. Xu, Phys. Chem. Chem. Phys. 16 (2014) 16891–16903.
[47] B. Weng, M.Q. Yang, N. Zhang, Y.J. Xu, J. Mater. Chem. A 2 (2014) 9380–9389.